

FORMATION AND DISSIPATION OF THE ELECTRON CLOUD*

M. A. Furman[†], LBNL, Berkeley, CA 94720, USA

Abstract

We present an understanding of the effect of various features of the secondary emission yield (SEY) and secondary emission spectrum on the formation and dissipation of the electron cloud (EC). This understanding is based on dedicated experimental studies at several storage rings and systematic benchmarks of simulations against these measurements.

INTRODUCTION

The electron-cloud effect (ECE) has been investigated experimentally, by simulations, and analytically at various storage rings for several years now [1]. Experimental investigations have made significant progress owing to the use of special-purposes devices such as retarding-field analyzers (RFA) installed at the APS, the PSR and BEPC [2], sweeping detectors at the PSR [3], and a strip detector at the SPS [4, 5]. These detectors allow the measurement of the electron flux and energy spectrum at the vacuum chamber wall, plus certain features of the EC distribution in the bulk. In addition, there is indirect evidence for the ECE at these and other storage rings from vacuum pressure measurements, tune spectra along the bunch train, bunch-by-bunch luminosity measurements, and BPM signals [4].

In this article we attempt to summarize our understanding of ECEs primarily at the APS, PSR and SPS based on the code POSINST [6], particularly the effects from features of the SEY and emission energy spectrum. The strength of the code is based on the embodiment of a detailed model for the secondary emission process [7]. We use as inputs to the simulation various laboratory measurements of the SEY and spectrum for various materials.

FORMATION

Primary mechanisms

Depending upon the type of machine, the EC is seeded by primary electrons from three main sources: photoelectrons, ionization of residual gas, and electrons produced by stray beam particles hitting the chamber wall. As these processes are essentially incoherent, it is customary to quantify them in terms of the number of primary electrons produced per beam particle per unit time, \dot{n}_{pr} , or per beam particle per unit length of beam traversal, n'_{pr} . These two are related by $\dot{n}_{pr} = n'_{pr} v_b$, where v_b is the speed of the beam.

We can estimate the various contributions to n'_{pr} from various other quantities. Photoelectrons are generated when synchrotron radiation emitted by the beam strikes the vacuum chamber. This is typically the dominant source of primary electrons for high-energy beams. The contribution from photoelectrons is given by

$$n'_{e(\gamma)} = Y_{\text{eff}} n'_{\gamma} \quad (1)$$

where n'_{γ} is the number of photons striking the vacuum chamber wall that are emitted per beam particle per unit length of trajectory, and Y_{eff} is the effective quantum efficiency, which must take into account factors such as the photon reflectivity of the surface, the photon angle of incidence on the surface, the photon energy spectrum, and the possible existence of an antechamber through which most photons can escape. Typical values for Y_{eff} are estimated in the range 0.05–1.

The contribution to primary electrons from residual gas ionization can be estimated from the gas density. The inverse of the mean free path for an ionization event by a particle traveling in a gas is given by $\rho \sigma_i$, where σ_i is the ionization cross-section. Expressing the gas density ρ in terms of the pressure and temperature yields

$$n'_{e(\text{ion})} [\text{m}^{-1}] = 3.3 \sigma_i [\text{Mbarn}] \times p_v [\text{Torr}] \times \frac{294}{T [\text{K}]} \quad (2)$$

where p_v is the vacuum pressure and T the temperature (implicit in this formula is the assumption that the ionization event yields a single electron). A typical value for σ_i is 2 Mbarns for a high-energy particle of unit charge [8]. Ionization of residual gas is typically the dominant source of primary electrons for relatively low-intensity hadron machines.

The contribution from stray beam particles striking the chamber walls is given by

$$n'_{e(\text{bpl})} = \eta_{\text{eff}} n'_{\text{bpl}} \quad (3)$$

where n'_{bpl} is the number of lost beam particles per beam particle per unit length of beam traversal, and η_{eff} is the effective electron yield per particle-wall collision (“bpl” stands for “beam-particle loss”). Beam particle losses is typically the dominant source of primary electrons for intense, low-energy proton storage rings such as spallation neutron sources.

The three above-mentioned types of primary electrons are produced with different spectra, and in different parts of the chamber. These details need to be taken into account in simulations. As for the time distribution of the electron production, it is reasonable to assume the proportionally

$$n'_e \propto \lambda_b(t) \quad (4)$$

* Work supported by the US DOE under contract DE-AC03-76SF00098.

[†] mafurman@lbl.gov

where n'_e represents any of the n' 's above, and $\lambda_b(t)$ is the beam line density at time t at a given azimuthal location in the ring. This proportionality is fairly obvious for the ionization electrons. As for photoelectrons, it is justified by noting that (a) only the incoherent photons radiated by the beam as it traverses a magnet are, in practice, significant, and (b) the photons, once radiated, remain substantially comoving with the beam until they hit the chamber wall. The same argument can be applied to the stray beam particles, regardless of the mechanism by which they are lost.

A basic quantity that is used to characterize the intensity of the EC is the electron line density as a function of time in a given section of the machine, $\lambda_e(t)$. Assuming that there is no antechamber, and that one can neglect the escape of the electrons at the endpoints of the given section, charge conservation implies that the rate of change in the number electrons in such a section is given by

$$\dot{N}_e = \underbrace{\dot{N}_{e(\gamma)} + \dot{N}_{e(ion)} + \dot{N}_{e(bpl)}}_{\text{primaries}} + \underbrace{\dot{N}_{sec} - \dot{N}_{col}}_{\text{net secondaries}} \quad (5)$$

where \dot{N}_{col} is the rate of electron-wall collisions, and \dot{N}_{sec} is the rate of secondary electrons produced in such collisions. Defining $\delta_{\text{eff}} = \dot{N}_{sec}/\dot{N}_{col}$ and dividing by the length of the section and multiplying by the electronic charge yields

$$\dot{\lambda}_e(t) = v_b n'_{pr} \lambda_b(t)/Z + (\delta_{\text{eff}} - 1)pI_{ew} \quad (6)$$

where Z is the beam-particle charge in units of e , p is the perimeter of the chamber cross section, $n'_{pr} = n'_{e(\gamma)} + n'_{e(ion)} + n'_{e(bpl)}$, and I_{ew} is the electron flux at the wall (units of current per unit area).¹ If electrons leave the chamber section through the antechamber or through the endpoints, these must be subtracted from the right-hand side of (6). This equation has not much predictive power, but its virtue lies in the fact that it relates several physical quantities that are either measured or simulated, and serves as a good check on calculations.

Secondary emission yield

In practice, it is often the case that the most important contribution to the EC is from secondary electron emission, embodied by δ_{eff} in Eq. (6). The secondary emission yield (SEY) function $\delta(E_0)$ is the average number of electrons emitted when an electron impinges on a surface at energy E_0 . It reaches a peak δ_{max} at an energy $E_0 = E_{\text{max}}$. A fairly detailed microscopic description of the secondary emission process is presented in Ref. 7, upon which we base the simulated examples discussed below.

To illustrate the sensitivity of the ECE to the SEY, we consider two sample measurements of δ and $d\delta/dE$, one for copper, the other one for stainless steel, both of which

¹In Eq. (6) Z appears explicitly because n'_{pr} is the electron production rate *per beam particle*, not *per unit charge*. I am indebted to M. Blaskiewicz for bringing this equation to my attention.

have $\delta_{\text{max}} \simeq 2.05$ and $E_{\text{max}} \simeq 300$ eV, that are discussed in detail in Ref. 7. Fig.1 shows a simulated example of the sensitivity exhibited by the EC line density to δ_{max} in a field-free region of the PSR. The two traces labeled $\delta_{\text{max}} = 1.5$ and 1.7 were obtained taking as basic input the stainless steel sample of Ref. 7 and scaling $\delta(E_0)$ down from its true peak value of 2.05 to either 1.5 or 1.7, respectively. It is apparent that the peak value of λ_e is almost an order of magnitude larger for $\delta_{\text{max}} = 1.7$ than for 1.5, while the plateau value in between bunches is a factor ~ 2 larger. An equally strong sensitivity is observed in the simulated electron-wall flux I_{ew} (not shown).

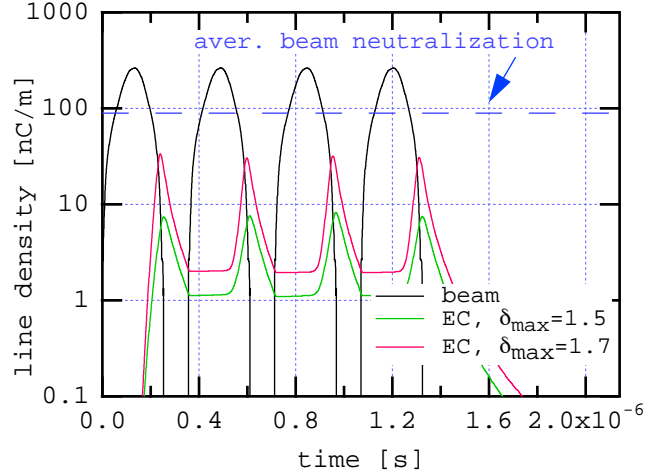


Figure 1: Simulated EC line density in a field-free region of the PSR for $\delta_{\text{max}} = 1.5$ and 1.7 . The beam, whose line density is also shown, has 5×10^{13} protons/bunch, and the primary electrons were assumed to be generated only from stray protons at a rate $n'_{e(bpl)} = 4.44 \times 10^{-6}$ e/m.

Secondary emission spectrum

A quantity closely related to δ is the emitted-energy spectrum of the secondary electrons, $d\delta/dE$ at given incident energy E_0 , where E is the emitted electron energy. The spectrum covers the region $0 < E \lesssim E_0$. The spectrum exhibits three fairly distinct main components: elastically reflected electrons, rediffused, and true secondaries [7]. The SEY is given by

$$\delta(E_0) = \int_0^{E_0} dE \frac{d\delta}{dE} \quad (7)$$

so that $\delta = \delta_e + \delta_r + \delta_{ts}$. The elastic electrons are emitted within a narrow peak (FWHM $\sim \pm 3$ eV) centered at $E \simeq E_0$. The rediffused electrons are emitted with a fairly uniform energy distribution in $\sim 50 < E < E_0$, and the true secondaries in a broad peak at $0 < E \lesssim 50$ eV. Depending upon various features of the storage ring considered, the three components can contribute differently to various aspects of the ECE. To illustrate this point,

we consider again the two above-mentioned sample measurements for copper and stainless steel. Even though δ_{\max} is almost the same for these two samples, the relative contributions of the three SEY components are quite different: for the stainless steel sample at $E_0 = 300$ eV, $(\delta_e, \delta_r, \delta_{ts}) \simeq (6\%, 37\%, 57\%)$ of δ , while for the copper sample, $(\delta_e, \delta_r, \delta_{ts}) \simeq (1\%, 9\%, 90\%)$ of δ . To illustrate the dependence of these relative ratios, we consider the simulated electron line density in an arc dipole in the LHC [6], shown in Fig. 2, and the power deposited by the electrons on the vacuum chamber walls, shown in Fig. 3.

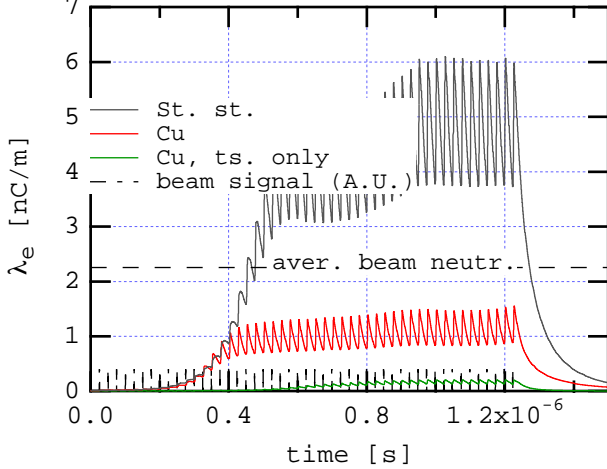


Figure 2: Simulated EC line density in an arc dipole magnet of the LHC assuming that the secondary emission off the chamber wall corresponds to a stainless steel sample, a copper sample, or a copper sample in which the elastic and rediffused electrons are artificially suppressed, i.e., true secondaries only (see text for details). In all three cases, $\delta_{\max} \simeq 2.05$ at $E_{\max} \simeq 300$ eV. In the first two, $\delta(0) \simeq 0.5$, while in the third, $\delta(0) = 0$. The beam, whose signal in arbitrary units is indicated by a dashed line, has $N = 1.05 \times 10^{11}$ protons/bunch, and the primary electrons were assumed to be generated only from the photoelectric process at a rate $n'_{e(\gamma)} = 6.3 \times 10^{-4}$ e/m.

The sensitivity exhibited in Figs. 2 and 3 can be explained from other features of the EC in this particular case (not shown in this article), and can be attributed to features of $\delta(E_0)$ and $d\delta/dE$. As it can be seen in Fig. 3, the peak power deposition occurs ~ 5 ns after the passage of the bunch, since this is the time it takes for the electrons kicked by the bunch to reach the chamber wall. The electrons that remain in the chamber for the balance of the inter-bunch gap may bounce off the walls once or a few times, and their average energy degrades with successive bounces. This degradation occurs primarily from the “conversion” of an incident electron into true secondary electrons, which are emitted with energies below ~ 50 eV. For the stainless steel sample, this energy degradation is slower than for the other cases because the electron emission spectrum has a relatively smaller true secondary component. Therefore,

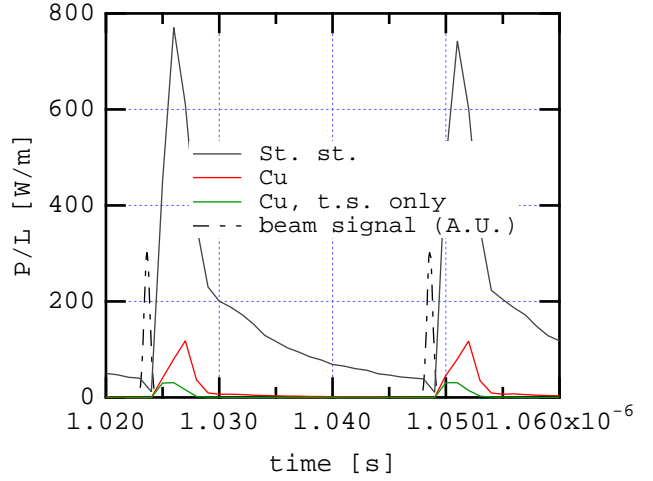


Figure 3: Simulated EC power deposition per unit length in an arc dipole magnet of the LHC for the same conditions as in Fig. 2. Only a short time interval (40 ns, with two bunch passages) is shown, chosen from the steady-state portion of the simulation.

since the energy of the slow electrons is relatively high, so is the corresponding SEY, hence these electrons also survive longer than in the other samples. Thus, when a new bunch comes along, it kicks a larger number of electrons into the wall for the stainless steel sample than for the others, leading to higher power deposition.

Beam-induced multipacting

An important mechanism for the EC formation is beam-induced multipacting (BIM) [9]. If a relativistic beam is composed of short, positively-charged bunches with N particles of charge Ze and bunch spacing s_b , a resonance condition occurs when the traversal time Δt of an electron across the chamber under the influence of one bunch equals s_b/c . If the impulse approximation is valid (bunch length $\ll s_b$), the resonance condition is $G = 1$, where G is defined by

$$G = \frac{ZNr_e s_b}{d^2} \quad (8)$$

where $r_e = e^2/mc^2 = 2.82 \times 10^{-15}$ m is the classical radius of the electron and d is the half-height of the vacuum chamber (or radius, if round). This definition of G is only pertinent to field-free regions and to dipole magnetic fields; in this latter case, $2d$ is the full size of the chamber along the magnetic field direction.

The condition $G = 1$ is necessary but not sufficient to lead to multipacting. The second necessary condition is $\delta_{\text{eff}} > 1$. When these two conditions are simultaneously valid, the EC density increases exponentially in time as successive bunches go by until a saturation is reached owing to space-charge forces. In addition to a rapid growth of the electron density, the electron-wall collision energy is typically high, leading to other phenomena such as rapid

and intense gas desorption and a possible catastrophic vacuum pressure increase.

BIM has been investigated in dedicated studies at the APS. Measurements have been obtained of I_{ew} and energy spectrum at the wall with RFAs, both for positron and electron beams [2, 10]. In these studies, a train of ten equally-spaced bunches of 2 mA/bunch were injected in the machine, and I_{ew} measured for various values of s_b in the range 1-128 RF buckets. Since the chamber cross-section is elliptical with semiaxes a, b and the measurements were done in a field-free region, the value of s_b for which $G = 1$, i.e., $s_b = d^2/Nr_e$, is not unique because d ranges in $b < d < a$. Simulations and measurements are in good agreement, and a clear bump is seen in I_{ew} when d is in this range [11].

A form of BIM is also seen for the case of very long bunches, such as the PSR, even though the electron traversal time Δt is much shorter than the bunch length. The phenomenon, “trailing-edge multipacting,” is observed in the trailing edge of the bunch [3]. In this case the resonance condition obtains when Δt equals the oscillation period of an electron in the potential well of the bunch. Simulations show that the multipacting (“prompt”) electrons are generated at the wall during the passage of the leading edge of the bunch, are temporarily trapped by the increasing depth of the potential well, and are then released as the depth decreases during the trailing edge. The phenomenon can be seen in Fig. 1; the electron flux at the wall (not shown) exhibits similar features as the density.

If the trailing edge of the bunch is artificially truncated keeping the bunch population fixed, trailing edge multipacting is effectively suppressed owing to the effective breaking of the resonance condition [12].

A weak ($\sim 20 - 30$ G) solenoidal field has been shown to be an effective means of controlling the ECE in B factories [1] by forcing the electrons to remain close to the walls of the chamber. However, a BIM condition arises if the bunch spacing s_b/c equals the electron cyclotron period in the solenoidal field [13].

DISSIPATION

If the beam is extracted from the machine, the EC dissipates. The rate of dissipation can yield important information about $\delta(E_0)$ for $E_0 \simeq 0$. The dissipation process also operates in the gap between bunches if the spacing s_b is significantly long, as is the case of the LHC. We consider a “blob” of N electrons, crossing the chamber in a time interval Δt . By definition of δ_{eff} , after one collision there will remain $N' = \delta_{\text{eff}}N$ electrons. If the electrons keep bouncing back and forth, after n collisions there will remain $N_n = Ne^{-n\Delta t/\tau}$ electrons, where τ is the decay time of the EC, hence we conclude that $\delta_{\text{eff}} = \exp(-\Delta t/\tau)$ [3, 14].

In the simplest estimation of Δt we assume that the electrons are created at the wall with a given kinetic energy E and that they cross the chamber along a diameter (if the chamber is round). If the EC is sufficiently dilute, we can

neglect the space-charge force hence the energy E is conserved, so that $\Delta t = (d/c) \times (2mc^2/E)^{1/2}$, hence

$$\delta_{\text{eff}} = \exp \left\{ -\frac{d}{c\tau} \sqrt{\frac{2mc^2}{E}} \right\} \quad (9)$$

where $2d$ is the full width of the chamber (or diameter if round), and m is the mass of the electron. In this analysis we have neglected the image forces, an approximation that simulations appear to support, as shown below. If one takes into account the energy-angle secondary emission spectrum, and the angular dependence of the SEY, an improved equation can be derived [14].

The development and deployment of a “sweeping electron detector” has allowed the measurement of the EC density in the bulk at the PSR [3]. These measurements show a fairly exponential decay of the EC with $\tau \simeq 200$ ns. Assuming a typical value $E = 4$ eV and $d = 5$ cm, one obtains $\delta_{\text{eff}} \simeq 0.5$.

In order to test the applicability of Eq. (9), we ran a simulation for the PSR using as input the above-mentioned model for stainless steel SEY, with $\delta(E_0)$ scaled so that $\delta_{\text{max}} = 1.7$. Results are shown in Fig. 4 for the line density. A similar simulation for the SPS in a region with a dipole field $B = 0.2$ T and rectangular chamber of half-sizes $(a, b) = (7.7, 2.25)$ cm, shows a slope of 170 ns.

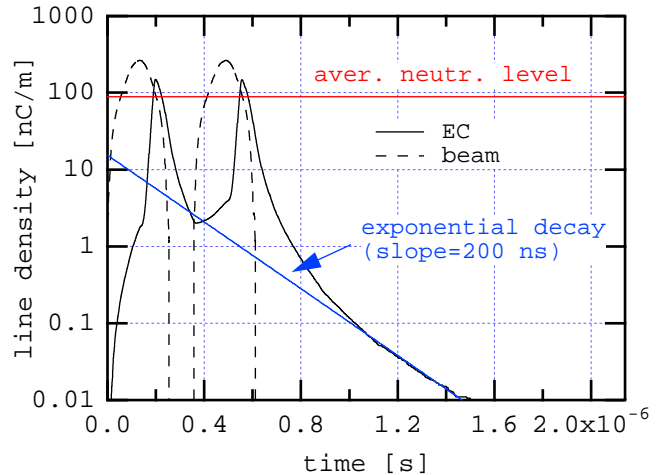


Figure 4: Line density for a field-free region of the PSR for $N = 5 \times 10^{13}$, $\delta_{\text{max}} = 1.7$, $\delta(0) = 0.4$, and an artificially high primary electron production rate $n'_{e(bpl)} = 4 \times 10^{-4}$ e/m.

One sees that the EC density indeed reaches an approximately exponential decay regime after a while (~ 400 ns) following beam extraction, with a slope in good agreement with Eq. (9). These results, combined with the simulation results for the electron-wall collision energy as a function of time (not shown), imply that the value of δ_{eff} extracted from Eq. (9) can be sensibly interpreted as $\delta(0)$.

CONDITIONING

Since the ECE can lead, in practice, to various performance limitations for intense beams, it is desirable to have as low a SEY as possible. The SEY of a given surface can be reduced (“conditioned”) by several mechanisms, including electron bombardment. Therefore, the ECE itself can lead to conditioning of the vacuum chamber (beam scrubbing).

Such conditioning has been observed at several storage rings including the SPS, where it is very effective, as evidenced by significant improvement of the vacuum pressure, *in situ* SEY measurements, and electron flux at the wall of a specialized detector [4] after \sim a few days of running. In addition, tests with TiVZr coatings indicate a full suppression of BIM once activated.

At the PSR it is observed that the prompt electron signal (ie., BIM electrons) is subject to conditioning, decreasing by factors of ~ 5 in certain regions of the machine after \sim a few weeks of running (albeit at low current). The conditioning effect is stronger for stainless steel than for TiN coatings, although it is location dependent. The prompt signal is also sensitive to the bunch population N ; it does not show signs of saturation up to $N \simeq 8 \times 10^{13}$. On the other hand, the swept-electron signal saturates for N beyond $\sim 5 \times 10^{13}$ and, significantly, the decay constant τ is roughly independent of N , location, conditioning state and surface material (stainless steel or TiN) [3]. Combining these observations with the results discussed above, one concludes that beam scrubbing effectively reduces δ_{\max} but leaves $\delta(0)$ unchanged. Although the PSR is the only storage ring that has produced evidence for this conclusion, it does not appear to be contradicted by experience at other machines. Nor does it contradict basic surface physics, because δ_{\max} and $\delta(0)$ are dominated by different processes: the former is dominated by true secondary electron production, while the latter is dominated by electron backscattering. Furthermore, recent measurements obtained for laboratory-conditioned Cu samples also show this effect: δ_{\max} for a sample is reduced from ~ 2 in the “as-received” state to ~ 1 in the fully scrubbed state, while $\delta(0)$ remains unchanged [15].

CONCLUSIONS

A consistent picture of the ECE is clearly emerging, particularly concerning the effects from the secondary electron emission. The understanding achieved is the result of dedicated experimental studies at various machines, especially the APS, SPS and PSR, combined with methodical simulation benchmarks. Recent progress in this understanding is leading to the elucidation of the effects from the three main components of the electron emission spectrum on different parts of the EC phase space, and its corresponding effects on EC density, electron flux and energy deposition on the vacuum chamber walls. Recent measurements indicate a differential beam scrubbing effect on the SEY: while the peak SEY is clearly reduced with electron bombardment, it

appears that the SEY below $\sim 5 - 10$ eV incident energy remains unchanged. If these measurements are confirmed, one can expect stronger ECEs than anticipated for beams with well-separated bunches.

ACKNOWLEDGMENTS

I am indebted to M. Blaskiewicz, M. Jiménez, R. Macek and F. Zimmermann for providing me important information relevant to the preparation of this talk. I am also grateful, for ongoing or past discussions and/or collaboration, to A. Adelmann, G. Arduini, M. Blaskiewicz, O. Brüning, Y. H. Cai, R. Cimino, I. Collins, O. Gröbner, K. Harkay, S. Heifets, N. Hilleret, J. M. Jiménez, R. Kirby, G. Lambertson, R. Macek, K. Ohmi, M. Pivi, G. Rumolo, and F. Zimmermann. I am grateful to NERSC for supercomputer support.

REFERENCES

- [1] Mini-Workshop on Electron-Cloud Simulations for Proton and Positron Beams E-CLOUD’02, CERN, Apr. 15-18 (CERN Yellow Report No. CERN-2002-001) 2002 <http://slap.cern.ch/collective/ecloud02/>
- [2] R.A. Rosenberg, K.C. Harkay, NIMPR A **453** (2000), 507-513.
- [3] R. Macek et al., these proceedings.
- [4] J. M. Jimenez, these proceedings.
- [5] F. Zimmermann et. al., these proceedings.
- [6] M. A. Furman and M. Pivi, Proc. EPAC02, Paris, June 3-7, 2002.
- [7] M. A. Furman and M. Pivi, PRSTAB **5**, 124404 (2002).
- [8] M. Reiser, *Theory and Design of Charged Particle Beams*, J. Wiley & Sons, 1994, Sec. 4.6.
- [9] O. Gröbner, Proc. 10th Intl. Accel. Conf., Serpukhov, 1977, pp. 277-282.
- [10] K. C. Harkay and R. A. Rosenberg, PRSTAB **6**, 034402 (2003).
- [11] M. A. Furman, M. Pivi, K. C. Harkay and R. A. Rosenberg, Proc. PAC01, Chicago, June 18-22, 2001, 679.
- [12] M. Pivi and M. A. Furman, these proceedings, paper RPPG024.
- [13] Y. H. Cai, M. Pivi, and M. A. Furman, Proc. PAC03, Portland, OR, May 12-16, 2003.
- [14] R. Macek, A. Browman, M. A. Furman and M. Pivi, to be published.
- [15] R. Cimino and I. Collins, Proc. DR2003 Damping Ring Workshop, Daresbury, UK, Jan. 27-29, 2003. <http://www.astec.ac.uk/conf/dampingring/>